





Cite this: *Phys. Chem. Chem. Phys.*,
2024, 26, 12661

Electronic structure and thermodynamic approaches to the prospect of super abundant vacancies in δ -Pu

Alexander Muñoz, * Ivana Matanovic,  Brendan Gifford, Sven Rudin,
Troy Holland and Travis Jones*

Super abundant vacancies (SAVs) have been suggested to form in the fcc phase of plutonium, δ -Pu, under a low-pressure hydrogen environment. Under these conditions, the vacancy concentration is proposed to reach 10^{-3} at% due to H trapping in vacancies lowering the effective vacancy formation energy. Previous density functional theory (DFT) results suggest that seven H atoms can be trapped in a single vacancy when a collinear special quasirandom magnetic structure is used to stabilize the δ phase, suggesting SAVs are a possible source of H stored in plutonium. In this report, we present DFT results for δ -Pu in the noncollinear 3Q magnetic state to study the formation of SAVs in mechanically stable δ -Pu. Together with these new simulations, we use publicly available computational and experimental data to provide further constraints on the physical conditions needed to thermodynamically stabilize SAVs in δ -Pu. Using several thermodynamic models, we estimate the vacancy concentrations in δ -Pu and discuss the limits of hydrogen driven formation of vacancies in δ -Pu. We find that, when hydrogen in the lattice is equilibrated with gaseous H_2 , the formation of SAVs in δ -Pu is unlikely and any excess vacancy concentration beyond thermal vacancies would need to occur by a different mechanism.

Received 5th February 2024,
Accepted 3rd April 2024

DOI: 10.1039/d4cp00534a

rsc.li/pccp

1 Introduction

The super abundant vacancies (SAV) model posits metal vacancy concentrations reach 10^{-3} at% in metal hydrides because of H trapping in vacancies.¹ While the occurrence of SAVs in metal hydrides has been observed,² it typically requires high H chemical potentials, often requiring GPa pressures, to stabilize the hydride phase at temperatures sufficient to drive vacancy formation and the appearance of an ordered vacancy phase. Electrodeposition has also been employed to grow metal hydride with SAVs.³ In many cases, vacancy ordered $L1_2$ SAV phases are thermodynamically favored in fcc metal hydrides because metal vacancy formation is exothermic.^{4,5} For instance, in PdH, the stable phase at room temperature is a Cu_3 Au-type ($L1_2$) structure with a Pd_3 Vac- H_4 stoichiometry rather than NaCl-type PdH, as observed through X-ray diffraction.² While this behavior commonly occurs in metal hydrides, SAVs do not typically form in metals with dissolved hydrogen owing to differences in the electronic structures of metal hydrides and metals.⁴ However, in the case of the fcc allotrope of plutonium (δ -Pu), anomalous hydrogen solubility data has been interpreted

as suggesting that 1–2 at% dissolved hydrogen may induce SAVs in the metal because the dissolved H lowers the vacancy formation energy.⁶ To date, however, it is unclear if the SAV mechanism operates in δ -Pu and whether SAVs form at low H chemical potentials before hydride (PuH_2) formation occurs.

Previous experimental work aimed to determine whether SAVs are present in δ -Pu with a low concentration of dissolved H. Experimental observations of lattice contractions when *ca.* 2 at% H is dissolved into δ -Pu at room temperature have been interpreted as evidence of SAVs in the metal because vacancy formation tends to reduce a metals lattice constant (*a*).^{8,9} While a vacancy concentration (x_v) of *ca.* 10^{-3} at% was estimated using such data, unfortunately, accurate estimation of x_v requires both $\frac{\Delta a}{a}$ and the macroscopic strain ($\frac{\Delta L}{L}$).¹⁰ However, the hydride radius is greater than the radius of the Pu atom, so, on H adsorption into the Pu complex, one should not expect a lattice contraction. Beyond such indirect measurements, however, vacancy concentrations in δ -Pu have also been measured by way of positron annihilation, which suggest x_v can reach as high as 0.1 at%. The same measurements indicate that these vacancies are filled with helium generated through α decay rather than H-induced SAVs.^{11–13} Beyond efforts to measure x_v , H diffusivity measurements show a concentration dependence in the dilute regime (<1 at%) that has been posited to demonstrate SAV

T-1: Physics and Chemistry of Materials, Theoretical Division, Los Alamos National Laboratory, Los Alamos, NM 87545, USA. E-mail: alexmunoz@lanl.gov, tejones@lanl.gov



formation in δ -Pu. The SAVs are assumed to trap dissolved H and therefore change the observed diffusivity. However, in all cases where SAV formation in δ -Pu is proposed, the dissolved H concentrations are far in excess of the solubility limit of *ca.* 10^{-7} at% found by extrapolating high temperature data with concentrations of *ca.* 1 at% known to precipitate the hydride.^{14,15} The experimental challenges associated with investigating SAV formation in δ -Pu have prompted researchers to perform computational investigations of possible SAV formation.

Using density functional theory (DFT), Taylor *et al.* showed multiple H can bind exothermically to vacancies in δ -Pu, with respect to gas phase H_2 .¹⁶ They went on to develop a statistical mechanical model to predict the hydrogen chemical potential, $\mu_{H_2}(T, p_{H_2})$, at which SAVs form based on their computed energetics. SAVs were found to become metastable at H chemical potentials sufficient to stabilize bulk PuH_2 showing there is no thermodynamic driving force for SAV formation in δ -Pu, though the authors speculated hydride formation may be slow enough to allow metastable SAV formation. However, this work employed a collinear special quasirandom magnetic structure to stabilize the δ phase of Pu, which may impact the computed energetics.¹⁷ While collinear antiferromagnetism results in a symmetry lowering of δ -Pu and mechanical instability, hence the common use of quasirandom magnetic structures, a newly proposed noncollinear 3Q structure restores the correct symmetry and eliminates mechanical instabilities.¹⁸ It is important to determine whether the mechanically stable 3Q magnetic structure will significantly change the DFT energetics of vacancy formation and H adsorption in δ -Pu, which is the subject of this effort. In this paper, we focus on the thermodynamic driving force for SAV formation, rather than the kinetic model. To do this, we develop thermodynamic models to establish whether H atoms drive SAV formation in δ -Pu and if vacancies can effectively trap dissolved H. These models are then parametrized using energetics computed for the 3Q

magnetic structure. We go on to set bounds on the energetics and chemical potentials required for SAV formation and test if published experimental and computational data fit within these bounds to demonstrate hydrogen does not induce SAV formation in δ -Pu.

2 DFT results

Computational results were obtained using DFT in the projector augmented wave method as implemented in the VASP package.^{19–21} We study δ -Pu with a noncollinear 3Q spin structure in which all structurally equivalent bonds have identical spin character in their bonding. This structure has been shown to remove the mechanical instability observed in previous collinear models of δ -Pu.¹⁸ Furthermore, elastic constants and phonons of δ -Pu calculated with the 3Q spin structure show the correct symmetry and lead to better agreement with experiment. Additionally, the DFT calculations with the noncollinear 3Q spin structure show a unique stiffening of most transverse phonon modes at contracted volumes, which leads to a negative thermal expansion as observed in experiment. The results in this work were obtained using the experimental lattice constant of 4.64 \AA .²² We used a $2 \times 2 \times 2$ conventional supercell with 32 atoms and the 3Q spin structure of δ -Pu. In this supercell, the distance between a defect and its mirror image is 9.28 \AA . The $4 \times 4 \times 4$ k -point mesh for this cell results in energy converged to less than 1 meV per atom and was used throughout this work. The electronic states were treated in the generalized gradient approximation using the exchange–correlation functional of Perdew *et al.* with first-order Methfessel–Paxton smearing and smearing width set to 0.2 eV.^{23,24} The cutoff energy for the plane wave basis was set to 500 eV.

To study the energetics of SAV formation, we began by computing the vacancy formation energy in δ -Pu with the

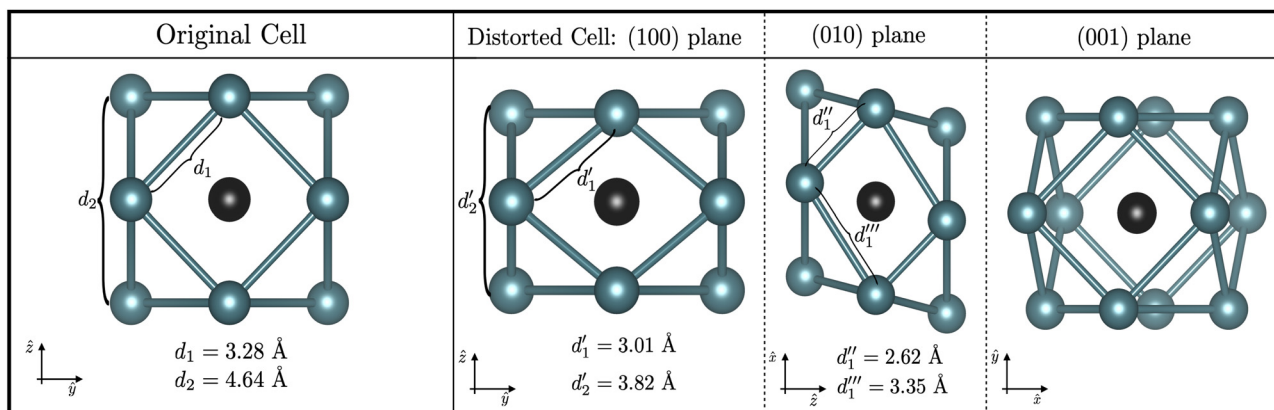


Fig. 1 Visualization in VESTA of the lattice centered on a vacancy in δ -Pu and the monoclinically distorted cell.⁷ Blue sites represent Pu atoms, and the black site is the vacancy in the center of the complex. Left panel: The original cell with labeled interatomic distances d_1 and d_2 . Right panels: View of the monoclinically distorted cell on the three faces of the complex. The (100) plane shows the compression in the [001] direction, or z direction in the figure, and the changes in the interatomic distances. The (010) plane shows the effect of the shearing in the [100] direction, x -direction in figure, and the compression in the [001] or z -direction. The shearing in the x -direction involves a displacement of five percent of the lattice constants. The (001) plane in the last panel shows the effect of the shearing.



undistorted octahedral symmetry as well as in the presence of a monoclinic distortion around the vacancy. For the monoclinic distortion, our initial geometry included displacing Pu atoms around the vacancy site. Four nearest neighbor atoms above (+z or [001] direction) the vacancy were compressed along the z-axis ([001] direction) and displaced along the x-axis (+x or [100] direction), while four atoms below (−z or [00 $\bar{1}$] direction) the vacancy were compressed along the z-axis with the same distortion along the x as the top atoms but in the opposite direction (−x or [$\bar{1}$ 00] direction), Fig. 1. The 3Q spin structure was initialized on all Pu atoms in the cell and allowed to relax. The monoclinic distortion affects the magnetic ground state as the bond equivalent directions in the lattice have shifted away from the Pu–Pu bond directions, Fig. 2. Distortions have been suggested to reduce the vacancy formation energy in δ -Pu, making the formation of SAVs more likely.¹⁷ We found that the monoclinic distortion does affect the vacancy formation energy but does not significantly affect the hydrogen adsorption energy (less than 0.05 eV). As a consequence, we compute the H adsorption using undistorted δ -Pu in the 3Q state for computational efficiency.

We compute the vacancy formation energy, the formation energy of hydrogen-vacancy complexes, and the binding energy per H atom in the noncollinear 3Q Pu structure using DFT. The binding energy of hydrogen atoms in an interstitial site of the pristine lattice is calculated as:

$$E_{\text{oct,H}}^f = \frac{1}{N_{\text{H,int}}} \left(E_{\text{Pu-H}_N} - E_{\text{Pu}} - \frac{N_{\text{H,int}}}{2} E_{\text{H}_2} \right), \quad (1)$$

where $E_{\text{Pu-H}_N}$ is the total energy of the Pu cell containing $N_{\text{H,int}}$ H atoms in the interstitial sites, E_{Pu} is the energy of the original supercell, and E_{H_2} is the energy of the hydrogen molecule, used as our hydrogen reference state. The H_2 energy was computed in VASP with the experimental bond length and a plane wave basis set cut-off of 500 eV.²⁵ The vacancy formation energy in

the absence of hydrogen is calculated using:

$$E_{\text{VH}_0}^f = E_{\text{Pu-VH}_0} - \frac{N_{\text{Pu}} - 1}{N_{\text{Pu}}} E_{\text{Pu}}, \quad (2)$$

where $E_{\text{Pu-VH}_0}$ is the total energy of the Pu cell containing a Pu vacancy, N_{Pu} is the number of Pu atoms in the cell, and E_{Pu} is the energy of the original Pu supercell. The formation energy of the hydrogen vacancy complex is:

$$E_{\text{VH}_N}^f = E_{\text{Pu-VH}_N} - \frac{N_{\text{Pu}} - 1}{N_{\text{Pu}}} E_{\text{Pu}} - \frac{N_{\text{VH}}}{2} E_{\text{H}_2}, \quad (3)$$

where $E_{\text{Pu-VH}_N}$ is the total energy of the Pu cell with a hydrogen-vacancy complex containing N_{VH} H atoms. The hydrogen binding energy in the vacancy can then be computed as:

$$E_{\text{H}}^b = E_{\text{VH}_N}^f - E_{\text{VH}_0}^f = E_{\text{Pu-VH}_N} - E_{\text{Pu-VH}_0} - \frac{N_{\text{VH}}}{2} E_{\text{H}_2}, \quad (4)$$

which we will then use to report the average binding energy in the vacancy per H atom:

$$E_{n\text{H}}^b = \frac{E_{\text{H}}^b}{N_{\text{VH}}}. \quad (5)$$

The values of the vacancy formation energies and binding energy per H atom as a function of hydrogen occupancy, N_{VH} , are reported in Table 1 and Fig. 3.

In running calculations with an fcc structure, with constrained magnetism, without constrained magnetism and with the distorted structure, we found that the vacancy formation energy ranges from 1.65–1.95 eV. The vacancy formation energy reported in Table 1 is the lowest value we obtained. This value comes from the use of the distorted cell with relaxed magnetic moment magnitudes and directions. The higher end of vacancy formation energy, 1.95 eV, comes from using the undistorted cell, creating a vacancy and constraining the remaining magnetic moments to the original 3Q structure. Our results in Table 1 show that Pu can accommodate 14 H atoms around a

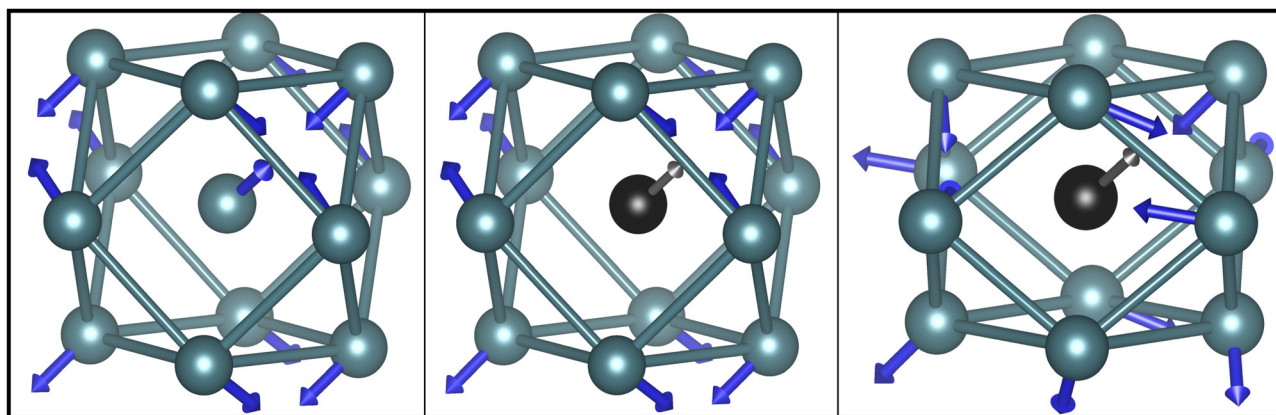


Fig. 2 The magnetic structure of δ -Pu and its undistorted and distorted vacancy complexes visualized in VESTA.⁷ Left: The 3Q magnetic state of δ -Pu where the blue spheres are Pu atoms, and the blue arrows are the directions of the magnetic moments on the Pu atoms. The 3Q state is identified by the noncollinear alignment of four Pu magnetic moments toward tetrahedral interstitial sites. Middle: The vacancy complex with the 3Q structure shows the vacancy in black in the center of the complex. The black arrow is the magnetic moment direction in the vacancy-free δ -Pu cell, preserved for visualization. Right: The monoclinically distorted cell relaxes the spins away from the 3Q structure. This relaxation of the spins reduces the vacancy formation energy.



Table 1 The vacancy formation energy ($E_{\text{VH}_0}^f$), the formation energy of the hydrogen vacancy complex ($E_{\text{VH}_n}^f$), the 95% confidence interval on the vacancy formation energy ($E_{\text{VH}_n}^f$ (u95%)), and the average binding energy per hydrogen atom (E_{H}^b) in eV evaluated for hydrogen occupancy $n = 0-14$ using a noncollinear 3Q spin structure of δ -Pu. We have included the 95% confidence interval as an estimate of our errors based on data accumulated by Medasani *et al.*^{26,27} Binding to the bulk interstitial sites in the noncollinear 3Q structure of δ -Pu yields adsorption energies of -0.20 eV and -0.47 eV for the tetrahedral and octahedral interstitial, respectively

N_{VH}	0	1	2	3	4	5	6	7	8	9	10	11	12	13	14
$E_{\text{VH}_0}^f$	1.65	1.11	0.55	0.00	-0.55	-1.10	-1.65	-1.85	-2.03	-2.22	-2.35	-2.64	-2.79	-3.03	-3.25
$\pm E_{\text{VH}_n}^f$ (u95%)	0.28	0.18	0.09	0.05	0.09	0.18	0.27	0.31	0.34	0.36	0.39	0.43	0.46	0.5	0.53
E_{H}^b		-0.54	-0.55	-0.55	-0.55	-0.55	-0.55	-0.50	-0.46	-0.43	-0.40	-0.39	-0.37	-0.36	-0.35

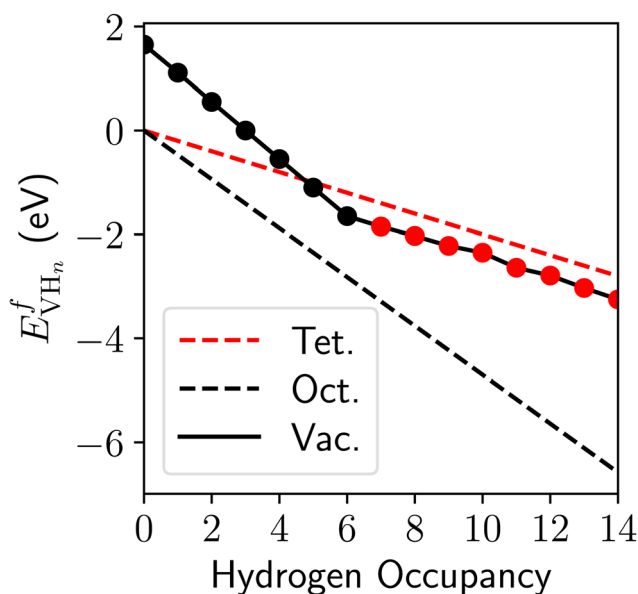


Fig. 3 The formation energy of vacancy-hydrogen complexes plotted against the H occupancy, N_{VH} , as calculated using the noncollinear 3Q structure of δ -Pu. The circles show the results of Table 1 with the black dots showing H going to octahedral interstitials around the vacancy and the red dots show the H entering tetrahedral interstitials.

Pu vacancy where the first six H atoms enter the octahedral interstitial sites around the vacancy, and the next eight H atoms enter the tetrahedral interstitial sites as shown in Fig. 4. On optimization of the geometry, we found that these H positions yield the minimum energy for the H-vacancy complexes. The formation of hydrogen-vacancy complexes become exothermic with four H atoms.

Successive placement of H atoms in the octahedral interstitial sites yields an adsorption energy of -0.55 eV, but on introducing H to the tetrahedral sites, the adsorption energy of H decreases with each additional H atom. In comparison, binding to the bulk interstitials in the noncollinear 3Q structure of δ -Pu, yields adsorption energies of -0.20 eV and -0.47 eV for the tetrahedral and octahedral interstitial, respectively. This demonstrates an enthalpic driving force for H atoms to bind around pre-existing vacancy sites until there are eight H atoms, at which point the eighth H atom will prefer to bind to the bulk octahedral interstitial sites.

The influence of the magnetic state on the vacancy formation energy and H adsorption is an open question in the

literature.^{28,29} The interplay of magnetic degrees of freedom and structural degrees of freedom creates a state space that makes *a priori* determination of the magnetic ground state difficult.¹⁷ As a test of this effect, we also computed the vacancy formation energy, and H adsorption energy using a collinear antiferromagnetic state with the monoclinically distorted cell. The vacancy formation energy is computed as 1.78 eV, and the H adsorption energy into the vacancy is computed as -0.48 eV. This indicates that further investigation into the magnetic structures effect on vacancy formation is necessary.

3 Thermodynamic analysis

In this report, we seek to develop simple statistical models to identify whether SAV formation is expected with slow hydride formation at 298 K in δ -Pu. We employ DFT total energies and assume dissolved H is mobile.³⁰ In Model 1, we compare dissolved and interstitial H with H trapped in vacancies to draw comparison to the H-charged Pu under vacuum measured in XRD. In model 2, we extend this analysis to study H-driven vacancy formation. The primary differences with the model proposed by Taylor *et al.* are the inclusion of configurational entropy for dissolved and interstitial H, and the study of metastable states by allowing high dissolved H concentrations. We compare phases at fixed H content to determine conditions where dissolved H can drive vacancy formation. In other words, we will determine the H partitioning, and whether SAV formation is possible in Pu that has been charged with $N_{\text{H}}\%$ H like in the experiments reported by Schwartz *et al.*⁸ This analysis is intended to discern between H free vacancy concentrations and the proposed SAVs at room temperature. In Model 3, we extend the model to include gas-phase H_2 .

3.1 Model 1

To develop this model, we begin by expressing the Helmholtz free energy in terms of energies from Table 1:

$$F(T, V, N_{\text{Pu}}, N_{\text{H}}) = E(V, N_{\text{Pu}}, N_{\text{H}}) + F^{\text{vib}}(T, V, N_{\text{Pu}}, N_{\text{H}}) + F^{\text{conf}}(T, V, N_{\text{Pu}}, N_{\text{H}}), \quad (6)$$

where E is the DFT total energy, F^{vib} is the vibrational contribution to the free energy, F^{conf} is the configurational contribution to the free energy, and N_{H} is the total number of H atoms in the system. The vibrational contribution to the free energy is:



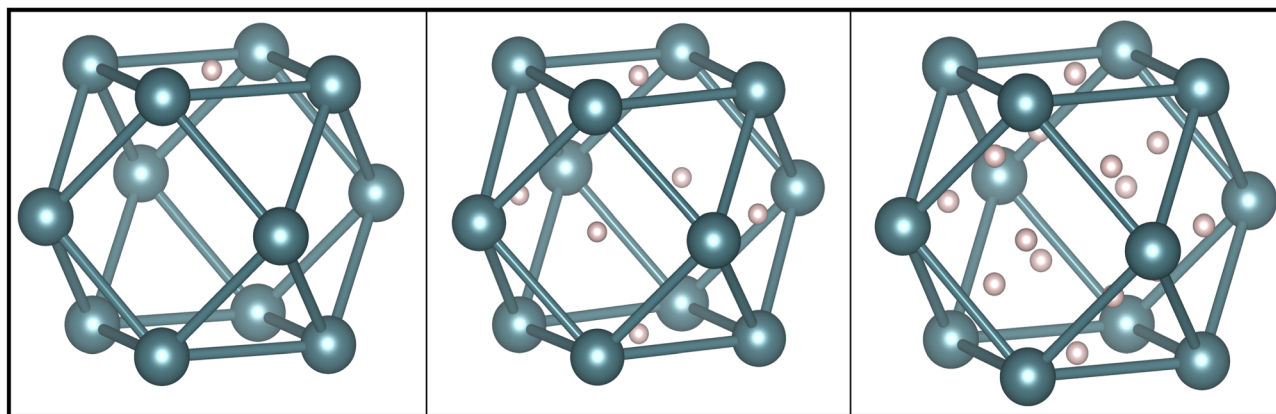


Fig. 4 Positions of H atoms adsorbed in the vacancy complex for one H atom, six H atoms, and 14 H atoms, visualized in VESTA.⁷ Left: The lowest energy configuration for one H atom is in an octahedral interstitial site neighboring the vacancy. Middle: The lowest energy configuration for six H atoms is for each H to occupy an octahedral interstitial. Right: After the first six H atoms, the H atoms will occupy the tetrahedral interstitials surrounding the vacancy.

$$F^{\text{vib.}}(T, V, N_{\text{Pu}}, N_{\text{H}}) = E^{\text{vib.}}(T, V, N_{\text{Pu}}, N_{\text{H}}) - TS^{\text{vib.}}(T, V, N_{\text{Pu}}, N_{\text{H}}), \quad (7)$$

where $E^{\text{vib.}}$ is the vibrational energy including the zero-point energy, and $S^{\text{vib.}}$ is the vibrational entropy. We ignore $S^{\text{vib.}}$ at room temperature and the zero-point energies are largely quenched in the solid.^{31,32}

Experimentally, we are concerned with constant pressure, so we can define the Gibbs free energy from the Helmholtz free energy:

$$G^{\text{vib.}}(T, p, N_{\text{Pu}}, N_{\text{H}}) = F^{\text{vib.}}(T, V, N_{\text{Pu}}, N_{\text{H}}) + pV(T, p, N_{\text{Pu}}, N_{\text{H}}). \quad (8)$$

Dimensional analysis shows the pV can be ignored since we are concerned with volumetric energies. The pV term contributes an energy per volume of:

$$\frac{pV}{V} = \text{atm} \text{Å}^3 \text{Å}^{-3} \approx 10^{-3} \text{meV} \text{Å}^{-3}. \quad (9)$$

A Pu atom is approximately 25Å^3 , which gives a pV contribution of 0.025meV , significantly less than the hundreds of meV associated with H adsorption. Therefore, at pressures around 100atm. , the enthalpy in the solid can be approximated by the total energy, which allows us to work directly with the data in Table 1.

With the free energy defined, we can determine if SAVs form with a given concentration of H in Pu by comparing the free

energy of a phase with interstitial H and a phase with H decorated vacancies. This model is illustrated in Fig. 5, where we can see that the problem amounts to identifying concentrations where the chemical potentials (μ_{H}) of various forms of stored H. Fig. 5 shows the case where interstitial H is equilibrated with 1H and 3H vacancy clusters.

From Table 1, the total energy of H can be reduced by 0.08eV by migrating from an interstitial site (-0.47eV) to a pre-existing vacancy (-0.55eV). This will, however, come at an entropic cost if the total number of lattice sites (N_{Pu}) is large compared to the vacancy concentration. The total energy cost required to form the vacancy will also reduce the tendency for migration from interstitials to vacancies, however, this enthalpic cost can be reduced by allowing multiple H to bind in the vacancy, which again comes with an entropic cost. Formation of the H vacancy moiety becomes exothermic, with respect to gas phase H_2 , when 4H are bound in the vacancy. However, if the H source is H dissolved in interstitial sites, as in our case, formation of the 4H vacancy complex is endothermic. Moreover, increasing the H content in the vacancy cannot result in exothermic H vacancy moiety formation with respect to H dissolved in the pristine lattice. Therefore, there is no enthalpic driving force for SAV formation from dissolved H in Pu.

We now turn to the configurational entropy as a potential driving force for SAV formation. For low concentrations, the

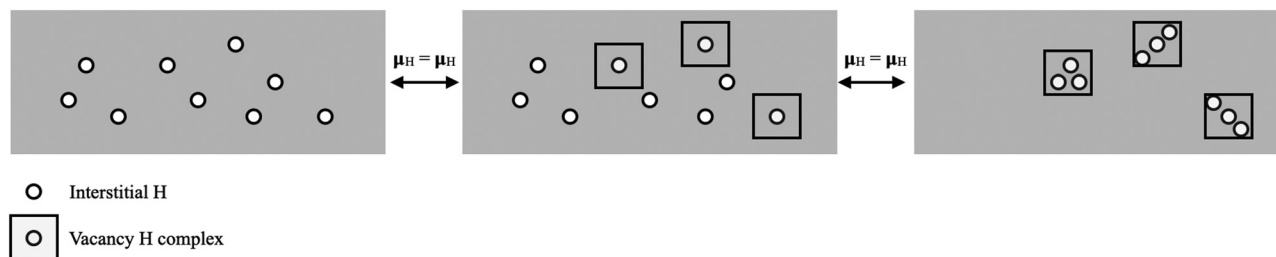


Fig. 5 Schematic of our modeling approach showing the equating of H chemical potential in different phases. Interstitial H is shown on the left, which, in this illustration, can equilibrate with 1H vacancy complexes (middle) or 3H vacancy complexes (right).



configurational entropy is written as the mixing entropy:

$$S^{\text{conf}} = -N_{\text{Pu}}k_B \sum_i x_i \ln x_i, \quad (10)$$

where x_i are the atomic fractions. The configurational entropy associated with placing N_V vacancies on N_{Pu} lattice sites is:

$$S_{VH_0} = -N_{\text{Pu}}k_B \left(\frac{N_{\text{Pu}} - N_V}{N_{\text{Pu}}} \ln \left(\frac{N_{\text{Pu}} - N_V}{N_{\text{Pu}}} \right) + \frac{N_V}{N_{\text{Pu}}} \ln \left(\frac{N_V}{N_{\text{Pu}}} \right) \right). \quad (11)$$

This entropic term drives vacancy formation despite the total energy/enthalpic cost associated with the process. The vacancy concentration is approximated as:

$$\frac{N_V}{N_{\text{Pu}}} = e^{\frac{-E_{VH_0}^f}{k_B T}}, \quad (12)$$

For δ -Pu, the vacancy formation energy of 1.65 eV yields a vacancy concentration of 1.84×10^{-28} at 298 K. Similarly, the number of ways of placing $N_{H,\text{int}}$ H atoms in N_{Pu} octahedral holes is:

$$S_{N_{H,\text{int}}} = -N_{\text{Pu}}k_B \left(\frac{N_{\text{Pu}} - N_{H,\text{int}}}{N_{\text{Pu}}} \ln \left(\frac{N_{\text{Pu}} - N_{H,\text{int}}}{N_{\text{Pu}}} \right) + \frac{N_{H,\text{int}}}{N_{\text{Pu}}} \ln \left(\frac{N_{H,\text{int}}}{N_{\text{Pu}}} \right) \right), \quad (13)$$

and similar expressions can be created to account for multiple H binding to an octahedral hole. Hydrogen favors octahedral holes in δ -Pu and the ratio of lattice sites to octahedral holes is 1-to-1.³³ Occupation of vacancies with N_{VH} hydrogen atoms gives rise to a configurational entropy related to the number of empty and H filled vacancies:

$$S_{VH_N} = -N_Vk_B \left(\frac{N_V - N_{VH}}{N_V} \ln \left(\frac{N_V - N_{VH}}{N_V} \right) + \frac{N_{VH}}{N_V} \ln \left(\frac{N_{VH}}{N_V} \right) \right). \quad (14)$$

The degeneracy of the binding sites in the vacancy has been ignored. Including 6 sites, for a single H binding will increase the computed vacancy concentrations by a factor of ten, which is irrelevant for our estimates.

With the configurational entropy, we rewrite the free energy:

$$G = \left(N_V E_{VH_0}^f - TS_{VH_0} \right) + \left(N_{VH} E_{nH}^b - TS_{VH_N} \right) + \left(N_{H,\text{int}} E_{\text{oct},H}^f - TS_{N_{H,\text{int}}} \right), \quad (15)$$

where E_{nH}^b is the adsorption energies per H atom in a vacancy, taken from Table 1. The first term in the free energy accounts for vacancy formation, the second term accounts for H filling vacancies, and the third term accounts for H dissolved in the pristine lattice.

To examine the super saturated case, where H concentrations are above those needed for PuH_2 precipitation, we want to understand how H will partition at fixed concentration. Assuming fixed total content of dissolved H, $N_H = N_{VH} + N_{H,\text{int}}$, we write the

free energy as:

$$G = \left(N_V E_{VH_0}^f - TS_{VH_0} \right) + \left(N_{VH} E_{nH}^b - TS_{VH_N} \right) + \left((N_H - N_{VH}) E_{\text{oct},H}^f - TS_{(N_H - N_{VH})} \right), \quad (16)$$

from which there is competition between dissolving H in interstitial and vacancy sites. To find the maximum vacancy concentration, we compute:

$$\left. \frac{\partial G}{\partial N_V} \right|_{N_{VH}, N_H} = 0 \quad (17)$$

to find the vacancy concentration that minimizes the free energy under fixed H content in interstitial and vacancy sites.

To determine the likelihood of additional kinetic traps we include a climbing image nudged elastic band calculation.^{34,35} We compute an activation energy of 0.9 eV using the climbing image nudged elastic band calculation. In conjunction with the low adsorption energy of H in vacancies relative to interstitial sites we do not expect additional kinetic traps. With single occupations of vacancies, the maximum Pu vacancy concentration is 1×10^{-27} for H concentrations below 10 at%. Comparing to the H-free vacancy concentration of 2×10^{-28} , we see that dissolved H can increase vacancy concentration, albeit marginally. The preceding result differs substantially from what is found if the configurational entropy of dissolved H is ignored and gas-phase H_2 is the hydrogen source. Dissolved H is mobile, so the vacancy H complexes compete with interstitial H, which will allow interstitial H to equilibrate with H trapped in vacancies. Thus, we rescale the vacancy formation energy as:

$$\frac{N_V}{N_{\text{Pu}}} = e^{\frac{E_{VH_0}^f - N_H \left(E_{nH}^b - E_{\text{oct},H}^f \right)}{k_B T}}, \quad (18)$$

where the thermodynamic reservoir of H is taken as dissolved H.⁸ This yields a vacancy concentration of 3×10^{-27} , far below the concentrations associated with SAVs. The configurational entropy cost associated with placing H in the small number of vacancies amounts to a factor of three reduction in vacancy concentration as compared to the estimate based on total energies alone. With single H occupancies, there is then a negligible for vacancy formation at 298 K.

Increasing the H content in vacancies does not increase the predicted vacancy concentrations. This should be expected from the data in Table 1: increasing the H concentration in a vacancy decreases its adsorption energy. We can illustrate this behavior using occupancies of 4H or 6H in the vacancies. Doing so allows the vacancy concentrations to reach maxima of 5×10^{-28} and 3×10^{-29} when configurational entropy is included, respectively. As before, ignoring the configurational entropy contribution of dissolved H slightly alters the predictions.

Using the total energies alone we can rescale the vacancy concentrations as:

$$\frac{N_V}{N_{\text{Pu}}} = e^{\frac{E_{VH_0}^f - 4 \left(E_{4H}^b - E_{\text{oct},H}^f \right)}{k_B T}}, \quad (19)$$



and

$$\frac{N_V}{N_{Pu}} = e^{-\frac{E_{VH_0}^f - 6(E_{6H}^b - E_{oct,H}^f)}{k_B T}}, \quad (20)$$

where E_{4H}^b and E_{6H}^b are the adsorption energy of H in the 4H and 6H vacancy clusters. These equations yield vacancy concentrations of 3.2×10^{-23} and 1.6×10^{-20} , respectively, at 298 K.

The predicted 4H vacancy cluster concentration increases by several orders of magnitude when the configurational entropy of H is ignored, and the 8H vacancy cluster concentration decreases by an order of magnitude when configuration entropy of H is ignored. While these changes are irrelevant for our overall analysis, they reflect the source of stabilization. The adsorption of H in the 4H vacancy cluster is marginally more exothermic than the interstitial H, so 4H vacancy cluster formation is driven by enthalpy. Conversely, the adsorption energy H in the 8H vacancy cluster is less than that of interstitial H, so 8H vacancy cluster formation is driven by the configurational entropy increase associated with placing a small amount of H in vacancies. In other words, placing 8H atoms in the vacancy increases the effective vacancy formation energy when those H atoms are equilibrated with interstitial H, while placing 4H atoms in a vacancy decreases the effective vacancy formation energy.

Note that in all the examined cases, the vacancy concentration remains closer to the 10^{-27} found for the H-free thermal vacancy concentration than the concentrations required for SAVs. This behavior is driven primarily by the small total energy differences between interstitial H and H in vacancies. Thus, using the appropriate thermodynamic reservoir of H shows SAV formation will not occur at 298 K for the magnetic state and defect used in this study.

3.2 Model 2

We now compute the equilibrium vacancy concentrations at room temperature in H_2 gas by considering the configurational entropy of dissolved H, thermal vacancies, and H trapped in vacancies. We will start with the chemical potential of dissolved H:

$$\mu_{diss,H} = E_{oct,H}^f - TS_{diss,nc} + k_B T \ln\left(\frac{x_H}{r - x_H}\right), \quad (21)$$

where we use $E_{oct,H}^f$ for an octahedral site in the lattice (-0.47 eV), which we assume to be equal to the enthalpy at the low pressures considered in this work, x_H is the concentration of dissolved H, and r is the number of interstitial sites per lattice site, which we will take to be 1 since we consider dissolution into octahedral holes. $S_{diss,nc}$ is the non-configurational entropy associated with dissolved H, which we take to be 0. The chemical potentials of the H vacancy complexes are:

$$\mu_{VH_N} = \frac{1}{N_{VH}} \left(E_{VH_N}^f - TS_{VH_N,nc} + k_B T \ln\left(\frac{x_V}{r - x_V}\right) + k_B T \ln\left(\frac{D}{N_{VH}}\right) \right), \quad (22)$$

where E_{VH_N} is the total energy of the vacancy hydrogen complex (Table 1), including H binding and vacancy formation energies.

$S_{VH_N,nc}$ is the non-configurational entropy associated with the vacancy H complexes, which we take to be 0; x_V is the concentration of vacancies, and r is the number of vacancies that can be made per lattice site, which we will take to be 1. In the above equation, H is only bound to vacancies, so the only entropy associated with distributing H atoms is in the final term, which accounts for possible degenerate binding sites in the vacancy. Since multiple H atoms can bind at each vacancy this entire expression must be divided by the number H atoms assumed to bind, N_{VH} . Setting the expression for $\mu_{diss,H}$ and μ_{VH} equal allows us to solve for the vacancy concentration as a function of H dissolved into the system.

This value is shown in Fig. 6 for the case of degenerate H adsorption in the vacancy for $1 \leq N_{VH} \leq 8$. Higher N_{VH} were not plotted for the sake of readability, but they sit below the lower level plotted here. Assuming the H induced, and thermal vacancy concentrations are independent, we find that below 5 at% dissolved H content, H will not induce vacancy formation above the level of normal thermal vacancies.

From Fig. 6, increasing the dissolved H content increases the concentration of H-induced vacancies as a power law as long as the dissolved H concentration remain low:

$$\ln(x_V) = N_{VH} \ln(x_H) + b_{N_{VH}}, \quad (23)$$

where N_{VH} is the number of H atoms in the vacancy. The intercept, $b_{N_{VH}}$, is a function of the total energies involved in the expression and the number H atoms bound to the vacancy under consideration:

$$b_{N_{VH}} = -\frac{E_{VH_N}^f - E_{oct,H}^f N_{VH}}{k_B T}. \quad (24)$$

This expression is valid for low concentrations of vacancies and dissolved H. From this power law relationship, however, the vacancy concentration will remain low when the dissolved H content is below 25% and that the vacancy-1H complex will be the most populated because of the $b_{N_{VH}}$ term.

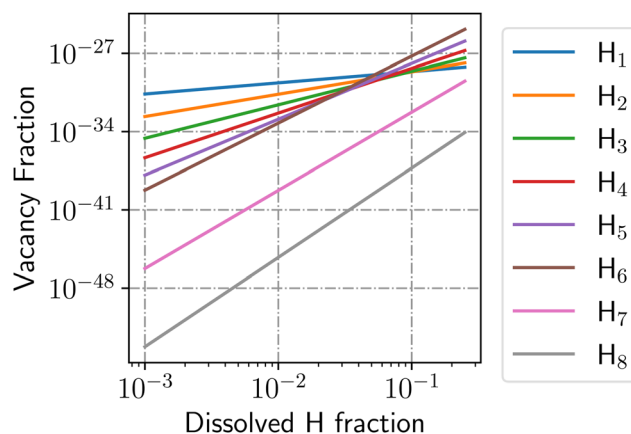


Fig. 6 Vacancy concentration in equilibrium with dissolved H at room temperature with 8-fold degenerate binding in the vacancy. The vacancy-1H complex exceeds the normal vacancy concentration when the dissolved H concentration exceeds 0.25 at%.



Equating eqn (21) and (22), we can see the vacancy concentration reaches only 10^{-28} for the vacancy-1H complex at $\text{PuH}_{0.25}$, which is far above the solubility limit.³⁶ Increasing the number of H atoms in the vacancy reduces the vacancy concentration because the heat of adsorption cannot offset the entropic penalty. The vacancy-3H complex has a concentration of only 10^{-30} at $\text{PuH}_{0.25}$. At $\text{PuH}_{0.25}$ we expect H will be distributed across interstitial sites with 10^{-28} of the H content trapped in vacancies. This gives a total vacancy concentration of 10^{-26} at $\text{PuH}_{0.25}$. While H induces vacancy formation already at 0.25 at% dissolved H, the vacancy concentration and total H stored in vacancies both remain negligible. Moreover, 0.25 at% may be above the solubility limit of H in Pu at 298 K, which we will now explore.¹⁴

3.3 Model 3

We connect to the gas phase chemical potential to address the vacancy concentration under fixed H_2 pressure by simply equating chemical potentials:

$$\mu_{\text{VH}_N}(T, p_{\text{H}_2}) = \frac{1}{2}\mu_{\text{H}_2, \text{gas}}(T, p_{\text{H}_2}). \quad (25)$$

Zero-point energy corrections are more likely to become important when comparing to a gas-phase reservoir. These were implicitly ignored in the preceding analysis, which is reasonable if the change in zero-point energy between dissolved H and H in vacancies is small, but this needs to be tested explicitly in the future. From experimental measurements of PuH_2 and PuD_2 it appears the zero-point energy is quenched in the solid; the difference in the heats of formation of PuH_2 and PuD_2 is equal to the differences in gas-phase zero point energies of H_2 and D_2 .³² Curiously, however, DFT gives values of 0.17 eV and 0.18 eV for the zero-point energy of H in the octahedral holes of Pu and the tetrahedral holes of PuH_2 .³⁷ While the two values are nearly identical, supporting our assumption that the zero-point energy in the solid will not change between sites, both values are larger relative to

the zero-point energy of $\frac{1}{2}\text{H}_{2, \text{gas}}$ (0.135 eV). An increase of H zero-point energy in the solid will reduce the predicted H-induced vacancy concentration and is at odds with experiment, so we will continue to assume the zero-point energy is quenched for H in the solid. For the gas-phase, however, we have:

$$\mu_{\text{H}_2, \text{gas}}(T, p_{\text{H}_2}) = E_{\text{H}_2} + \tilde{\mu}_{\text{H}_2}(T, p_0) + k_B T \ln\left(\frac{p}{p_0}\right) + ZPT, \quad (26)$$

where E_{H_2} is the total energy of H_2 from DFT, $\tilde{\mu}_{\text{H}_2}(298 \text{ K}, 1 \text{ atm}) = -0.32 \text{ eV}$ and $\tilde{\mu}_{\text{D}_2}(298 \text{ K}, 1 \text{ atm}) = -0.36 \text{ eV}$, is the enthalpic and entropic correction to the total energy at 298 K.⁴ ZPT is the experimental zero-point energy of H_2 (0.27 eV) and D_2 (0.19 eV).²⁵

The $k_B T \ln\left(\frac{p}{p_0}\right)$ term accounts for changes in pressure assuming H_2 behaves as an ideal gas, where p_0 is standard pressure. This approach is shown schematically in Fig. 7, where gas-phase H_2 fixes the H chemical potential.

If we ignore changes in entropic effects in the solid phases, the allowed range of chemical potential for H dissolved in Pu will be bound by the heat of formation of PuH_2 . That is, the decomposition pressure of PuH_2 is fixed by:

$$\mu_{\text{H}_2, \text{gas}}(298 \text{ K}, p_{\text{H}_2}) \approx \Delta H_{\text{PuH}_2}, \quad (27)$$

where ΔH_{PuH_2} is the heat of formation of PuH_2 , which can be measured or computed. We can also employ an extrapolation of experimentally measured decomposition pressure. This gives three approximations to the decomposition pressure:

- Experimental ΔH of PuH_2 :³² $p_{\text{PuH}_2} \approx 3 \times 10^{-27} \text{ atm}$
- Theoretical ΔH computed with DFT: $p_{\text{PuH}_2} \approx 5 \times 10^{-29} \text{ atm}$.
- Pressure extrapolated from the measured decomposition temperature:³² $p_{\text{PuH}_2} \approx 5 \times 10^{-21} \text{ atm}$.

The choice to use several approaches is motivated by the possibility that using the DFT result will give error cancellation with the computed H adsorption energies. However, as capturing

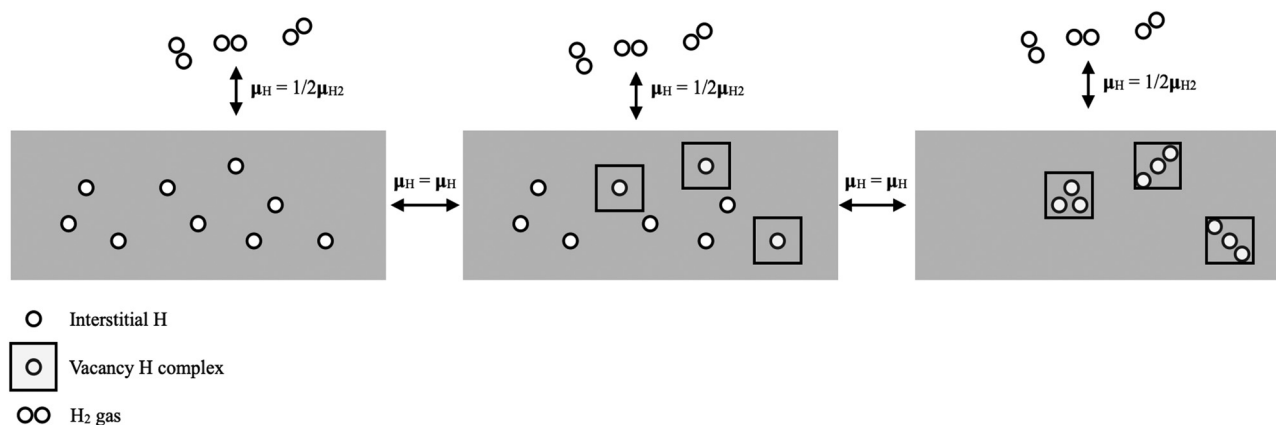


Fig. 7 Schematic of modeling showing the equating of H chemical potential in different phases. Interstitial H is shown on the left, which, in this illustration, can equilibrate with 1H vacancy complexes (middle) or 3H vacancy complexes (right), all of which have the H chemical potential fixed by gas phase H_2 .

Table 2 The H concentration ($\frac{N_H}{N_{Pu}}$) computed at the decomposition pressures of PuH₂ at 298 K under different assumptions: DFT ΔH uses heat of formation of PuH₂ from DFT; Exp ΔH for PuH₂ is from Mullen;³² Extrapolated decomposition pressure uses decomposition pressure extrapolated from high T data.³² The 6-fold degeneracy for H adsorption into octahedral vacancies has been included. Note the 3Q structure predicts a thermal vacancy concentration of 7×10^{-27} and was computed at the experimental lattice constant with $E_{VH_0}^f = 1.65$ eV

	DFT ΔH	Exp. ΔH	Extrap. decomp.
Vac.-H ₁ complex	9×10^{-19}	1×10^{-21}	2×10^{-18}
Dissolved H	4×10^{-4}	6×10^{-7}	8×10^{-4}
Vac.-D ₁ complex	9×10^{-19}	6×10^{-21}	6×10^{-18}
Dissolved D	4×10^{-4}	3×10^{-6}	3×10^{-4}
Vac.-H ₁ complex (3Q)	7×10^{-35}	6×10^{-34}	7×10^{-31}
Dissolved H (3Q)	2×10^{-7}	2×10^{-6}	2×10^{-3}

the structure of the dihydride and metallic forms of plutonium require different approximate Hamiltonians in DFT, it is unclear such error cancellation will occur. Thus, we include the measured heat of formation. Finally, extrapolation of the decomposition pressure to 298 K offers the most direct route, but relies on extrapolating from temperatures all of which are above 673 K. The resulting H-induced vacancy concentrations are summarized in Table 2 and can be seen to vary by up to 4 orders of magnitude but remain below the thermal vacancy concentration of 2.7×10^{-27} at 298 K. Table 2 also shows the maximum concentration of dissolved H is predicted to be 10^{-7} to 10^{-4} at 298 K, which is above the 10^{-9} extrapolated from experiment but below the 10^{-3} predicted from a DFT parameterized lattice gas model.³⁷

Below pressures where dihydride forms the H-vacancy complexes reach a concentration of 10^{-35} – 10^{-30} , depending on what decomposition pressure is employed. This behavior is

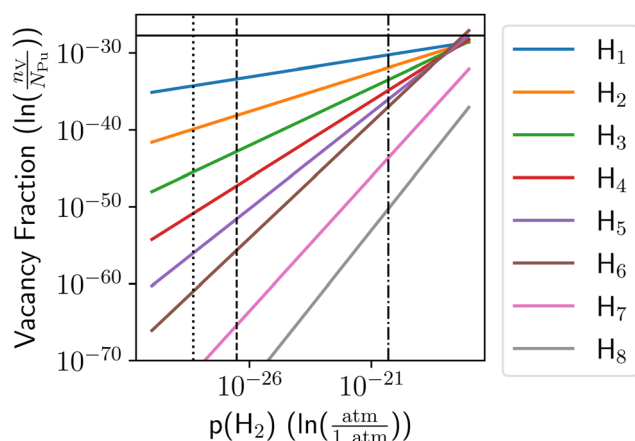


Fig. 8 Vacancy concentration vs. gas phase H₂ pressure at 298 K. Zero-point energies of the solid are taken as zero, while the experimental value of the zero-point energy for gas-phase H₂ was employed. The dashed vertical line shows the decomposition pressure of PuH₂ found from the experimental heat of formation of PuH₂ ($\mu_{H_2, \text{gas}} = \Delta H_{\text{PuH}_2}$), the dotted line is the decomposition pressure of PuH₂ found from the DFT heat of formation of PuH₂ ($\mu_{H_2, \text{gas}} = \Delta H_{\text{DFT}}$), and the dashed-dotted line is the decomposition pressure extrapolated from experimental decomposition pressures.³⁷

shown in Fig. 8, where the vertical lines show the different possible dihydride decomposition pressures, and the horizontal line shows the H-free thermal vacancy concentration. In all cases, the total concentration of H-vacancy complexes is less than the concentration of thermal vacancies, suggesting no SAV formation occurs. A 10^{-3} at% vacancy concentration would require quasi-equilibration with 4×10^{-11} atm H₂, which would yield a stoichiometry of PuH_{0.99} assuming the energetics from Table 1. The model presented here will not be valid under those conditions and there is no evidence supporting such super-saturation of Pu metal with H can occur. Thus, SAVs will not form under equilibration with gas-phase H₂ at 298 K.

It is worth considering the DFT error in energy required to reach a 10^{-3} at% vacancy concentration for the vacancy complex with one H atom at 298 K. This is the limiting error, and it could be in the vacancy formation energy, the adsorption energy of H at a vacancy, or a combination of the two. It will depend on the method used to compute the dihydride dissociation energy and runs from 0.76 eV to 0.90 eV. That is, the vacancy formation energy must be overestimated by 0.76 eV to 0.90 eV, or the adsorption energy of H must be underestimated by 0.76 eV to 0.90 eV, or a combination of overestimated vacancy formation energy and underestimated H trapping energy must total 0.76 eV to 0.90 eV. Considering that the computed heat of formation of PuH₂ differs from the measured value by 0.05 eV per H atom, an error above 0.76 eV per atom is unlikely. This value also exceeds the MAE found for energies computed with the PBE functional.^{38–40} As a more robust measurement of the error, we include the 95% confidence interval for the heat of formation to our analysis which yields 0.17 eV per atom.²⁶ The combination of the shift in the vacancy formation energy and the resultant change of the dissociation pressure is insufficient to obtain the vacancy concentrations associated with SAVs.

The absence of SAVs in δ -Pu is in line with expectations, where unlike in the case of metal hydrides, metals tend not to form SAVs as metal-metal bonding is typically stronger than the metal-hydrogen bonding found in the hydrides. As a demonstration, we consider PuH₂ in the 3Q magnetic state. The magnetism of PuH₂ and related materials is a matter of debate with ferromagnetism, collinear antiferromagnetism and noncollinear magnetism being actively discussed.^{15,41–44} An in-depth study of the magnetism of PuH₂ is beyond the scope of this study, but warrants further investigation. Consistent with this view, the Pu vacancy formation energy in PuH₂ in the 3Q magnetic state is 0.21 eV, significantly lower than the 1.65 eV found in δ -Pu, and with a thermal vacancy concentration on the order of 10^{-4} , the bulk PuH₂ hydride falls much closer to the SAV regime.

4 Conclusions

Super abundant vacancies (SAVs) have been suggested to form in δ -Pu under a low-pressure hydrogen environment. In this report, we presented DFT results for δ -Pu in the noncollinear



3Q magnetic state to study the formation of SAVs. With publicly available experimental data, we provide further constraints on the physical conditions needed to thermodynamically stabilize SAVs in δ -Pu. In developing several thermodynamic models, we estimate the vacancy concentrations in δ -Pu and discuss the limits of hydrogen driven formation of vacancies. We find that, when hydrogen in the lattice is equilibrated with gaseous H_2 , the formation of SAVs in δ -Pu is unlikely and any excess vacancy concentration beyond thermal vacancies would need to occur by a different mechanism. Without H, the room temperature vacancy concentration is predicted to be 2.7×10^{-27} . Under conditions where PuH_2 forms the maximum vacancy concentration may reach 10^{-25} in δ -Pu due to H incorporation. In all other cases, H incorporation does not increase the vacancy concentration at room temperature.

Predicted maximum concentrations of dissolved H at 298 K range between 10^{-7} to 10^{-4} at% and these lower pressures will have fewer H induced vacancies. While this range is large, it is within the bounds reported based on experimental extrapolation (10^{-9}) and lattice gas model results (10^{-3}).³⁷ However, our analysis of metastable phases showed that even if dissolved H concentrations reach above 2 at%, an SAV phase will not form in δ -Pu. In summary, there is no evidence that vacancies are a non-negligible source of stored H in δ -Pu, and H does not induce significant vacancy formation in the metal at 298 K. However, other defect structures with noncollinear magnetism may be able to push the metal closer to the SAV regime.

Conflicts of interest

There are no conflicts to declare.

Acknowledgements

The authors would like to acknowledge the LDRD project number 20230202DR. This research used resources provided by the Los Alamos National Laboratory Institutional Computing Program, which is supported by the U.S. Department of Energy National Nuclear Security Administration under Contract No. 89233218CNA000001.

Notes and references

- Y. Fukai and N. Okuma, *Phys. Rev. Lett.*, 1994, **73**, 1640–1643.
- Y. Fukai, *Phys. Scr.*, 2003, **11**.
- Y. Fukai, M. Mizutani, S. Yokota, M. Kanazawa, Y. Miura and T. Watanabe, *J. Alloys Compd.*, 2003, 270–273.
- C. Zhang and A. Alavi, *J. Am. Chem. Soc.*, 2005, **127**, 9808–9817.
- Y. Fukai, *J. Alloys Compd.*, 1995, **231**, 35–40.
- Plutonium Handbook*, ed. D. L. Clark, D. A. Gleeson and R. J. H. Jr., American Nuclear Society, 2nd edn, 2019, vol. 2.
- K. Momma and F. Izumi, *J. Appl. Crystallogr.*, 2011, **44**, 1272–1276.
- D. Schwartz, S. Richmond, C. Taylor, A. Smith and A. Pugmire, *Plutonium Futures-The Science*, 2014.
- D. S. Schwartz, S. Richmond, A. I. Smith, A. Costello and C. D. Taylor, *MRS Online Proc. Libr.*, 2012, **1444**, 183–188.
- R. O. Simmons and R. W. Balluffi, *Phys. Rev.*, 1960, **117**, 52–61.
- C. Colmenares, R. Howell, D. Ancheta, T. Cowan, H. Hanafee and P. Sterne, *First positron annihilation lifetime measurement of Pu*, Lawrence Livermore National Laboratory, Technical Report, 1996.
- R. Howell, L. Summers, D. Ancheta, T. Cowan, J. Hanafee and P. Sterne, *Positron annihilation study of age-induced defect structures in Plutonium*, Lawrence Livermore National Laboratory, Technical Report, 1997.
- P. A. Sterne and J. E. Pask, *AIP Conf. Proc.*, 2003, **673**, 205–206.
- T. H. Allen, *The solubility of hydrogen in plutonium in the temperature range 475 to 825 degrees centigrade*, Rocky flats, Inc., technical report, 1991.
- J. W. Kim, E. D. Mun, J. P. Baiardo, A. I. Smith, S. Richmond, J. Mitchell, D. Schwartz, V. S. Zapf and C. H. Mielke, *J. Appl. Phys.*, 2015, **117**, 053905.
- C. D. Taylor, M. F. Francis and D. S. Schwartz, *Phys. Rev. B: Condens. Matter Mater. Phys.*, 2014, **89**, 214114.
- S. C. Hernandez, F. J. Freibert, R. G. Hoagland, B. P. Uberuaga and J. M. Wills, *Phys. Rev. Mater.*, 2018, **2**, 085005.
- S. P. Rudin, *J. Nucl. Mater.*, 2022, **570**, 153954.
- P. E. Blöchl, *Phys. Rev. B: Condens. Matter Mater. Phys.*, 1994, **50**, 17953–17979.
- G. Kresse and J. Furthmüller, *Phys. Rev. B: Condens. Matter Mater. Phys.*, 1996, **54**, 11169–11186.
- G. Kresse and D. Joubert, *Phys. Rev. B: Condens. Matter Mater. Phys.*, 1999, **59**, 1758–1775.
- F. H. Ellinger, *JOM*, 1956, **8**, 1256–1259.
- J. P. Perdew, K. Burke and M. Ernzerhof, *Phys. Rev. Lett.*, 1996, **77**, 3865–3868.
- M. Methfessel and A. T. Paxton, *Phys. Rev. B: Condens. Matter Mater. Phys.*, 1989, **40**, 3616–3621.
- K. K. Irikura, *J. Phys. Chem. Ref. Data*, 2007, **36**, 389–397.
- B. Ruscic, *Int. J. Quantum Chem.*, 2014, **114**, 1097–1101.
- B. Medasani, M. Haranczyk, A. Canning and M. Asta, *Comput. Mater. Sci.*, 2015, **101**, 96–107.
- M. Huda and A. Ray, *Phys. B*, 2004, **352**, 5–17.
- M. T. Curnan and J. R. Kitchin, *J. Phys. Chem. C*, 2014, **118**, 28776–28790.
- C. D. Taylor, S. C. Hernandez, M. F. Francis, D. S. Schwartz and A. K. Ray, *J. Phys.: Condens. Matter*, 2013, **25**, 265001.
- R. Nazarov, T. Hickel and J. Neugebauer, *Phys. Rev. B: Condens. Matter Mater. Phys.*, 2014, **89**, 144108.
- R. N. R. Mulford and G. E. Sturdy, *J. Am. Chem. Soc.*, 1955, **77**, 3449–3452.
- R. G. Mullen and N. Goldman, *J. Chem. Phys.*, 2021, **155**, 234702.
- G. Henkelman and H. Jónsson, *J. Chem. Phys.*, 2000, **113**, 9978–9985.



- 35 G. Henkelman, B. P. Uberuaga and H. Jónsson, *J. Chem. Phys.*, 2000, **113**, 9901–9904.
- 36 S. Richmond, J. S. Bridgewater, J. W. Ward and T. H. Allen, *IOP Conf. Ser.: Mater. Sci. Eng.*, 2010, **9**, 012036.
- 37 R. G. Mullen and N. Goldman, *J. Phys. Chem. C*, 2020, **124**, 20881–20888.
- 38 J. Wellendorff, T. L. Silbaugh, D. Garcia-Pintos, J. K. Nørskov, T. Bligaard, F. Studt and C. T. Campbell, *Surf. Sci.*, 2015, **640**, 36–44.
- 39 L. Vega, J. Ruvireta, F. Viñes and F. Illas, *J. Chem. Theory Comput.*, 2018, **14**, 395–403.
- 40 P. Janthon, S. M. Kozlov, F. Viñes, J. Limtrakul and F. Illas, *J. Chem. Theory Comput.*, 2013, **9**, 1631–1640.
- 41 J. T. Pegg, A. E. Shields, M. T. Storr, A. S. Wills, D. O. Scanlon and N. H. de Leeuw, *Phys. Chem. Chem. Phys.*, 2018, **20**, 20943–20951.
- 42 T. Smith, S. Moxon, D. J. Cooke, L. J. Gillie, R. M. Harker, M. T. Storr, E. L. da Silva and M. Molinari, *Crystals*, 2022, **12**, 1499–1512.
- 43 S. Li, Y. Guo, X. Ye, T. Gao and B. Ao, *Int. J. Hydrogen Energy*, 2017, **42**, 30727–30737.
- 44 T. Muromura, T. Yahata, K. Ouchi and M. Iseki, *J. Inorg. Nucl. Chem.*, 1972, **34**, 171–173.

